Quantum Microwave Radiometry with a Superconducting Qubit

Zhixin Wang,[1,*] Mingrui Xu,[2] Xu Han,[2,‡] Wei Fu,[2] Shruti Puri,[1] S. M. Girvin,[1] Hong X. Tang,[2] S. Shankar,[1,§] and M. H. Devoret[1,†]

[1]Department of Applied Physics and Physics, Yale University, New Haven, Connecticut 06520, USA
[2]Department of Electrical Engineering, Yale University, New Haven, Connecticut 06520, USA

(Received 9 November 2019; accepted 29 March 2021; published 5 May 2021)

The interaction of photons and coherent quantum systems can be employed to detect electromagnetic radiation with remarkable sensitivity. We introduce a quantum radiometer based on the photon-induced dephasing process of a superconducting qubit for sensing microwave radiation at the subunit photon level. Using this radiometer, we demonstrate the radiative cooling of a 1 K microwave resonator and measure its mode temperature with an uncertainty ∼0.01 K. We thus develop a precise tool for studying the thermodynamics of quantum microwave circuits, which provides new solutions for calibrating hybrid quantum systems and detecting candidate particles for dark matter.

DOI: 10.1103/PhysRevLett.126.180501

Historically, radiometry experiments—measurements of the intensity of radiation—revealed the first invisible band of the electromagnetic spectrum [1], unveiled the law of radiative energy transfer [2,3], provoked the genesis of quantum theory [4,5], and provided the landmark evidence for the Big Bang model of the Universe [6–8]. Contemporarily, a number of investigations in mesoscopic [9] and particle physics [10] are demanding microwave radiometry with single-photon sensitivity. In this Letter, we present a quantum-limited radiometry protocol based on the photon-induced dephasing of a superconducting qubit. By converting a small photon population to qubit coherence times, this mechanism is particularly suited for detecting microwave radiation beyond the Rayleigh–Jeans regime where single-photon energy exceeds the energy of thermal fluctuations.

A classical microwave radiometer [11] typically consists of a radio receiver followed by a square-law detector. In reality, receiving circuits always add noise to the antenna radiation. This system noise, represented by a system temperature T_{sys} limits the sensitivity of a radiometer [12]. A common practice for reducing T_{sys} is to equip the receiver with cryogenic low-noise amplifiers [13–15]. Alternatively, one can directly detect quantum radiation with novel microwave sensors. For instance, in circuit quantum electrodynamics (cQED) systems [16–19], one can deduce the coherent [20] or white thermal-photon population [21–27] of a microwave cavity from qubit coherence times—an effect known as photon-induced qubit dephasing [28–30]. This method has been applied to extract the thermal populations of qubit-readout cavities with a precision of $\sim 10^{-4}$ [27]. However, cQED radiometers have not yet been employed to probe external radiative sources with pulsed emission or colored spectra.

A frequently encountered type of thermal radiator is an electrical resonator at finite temperature, whose output field has a Lorentzian power spectral density. Consider a resonator mode at frequency f coupled with rate κ_c to a transmission line at temperature T_c and with rate κ_i to an internal dissipative mechanism thermalized to a bath at $T_i > T_c$. The average thermal population of this resonator mode is $\bar{n} = (\kappa_c \bar{n}_c + \kappa_i \bar{n}_i)/(\kappa_c + \kappa_i)$, in which $\bar{n}_{c(i)} = (e^{hf/k_B T_{c(i)}} - 1)^{-1}$. Radiative cooling ($\bar{n} \to \bar{n}_c$) is manifested if $\kappa_c \gg \kappa_i$, namely, when the resonator is overcoupled to a colder external bath. The same thermodynamic principle underlies nocturnal cooling on cloudless nights [31,32] when the Earth's surface, in contact with the 300 K atmosphere, is cooled by radiative emission into the cold bath of space, whose temperature of 3 K is set by the cosmic microwave background radiation. In this work, to test our qubit radiometer, we measured the thermal radiation from a 1 K microwave resonator and demonstrated its radiative cooling by coupling it to a ∼0.1 K external bath. Noise analysis yields $T_{\mathrm{sys}} = 0.31\ \mathrm{K} \sim hf/2k_B$, which is dominated by dissipation and thermal leakage at low temperatures. It is a factor of 2 below the minimum output noise energy hf of an ideal quantum-limited phase-preserving linear amplifier, which includes both the amplified vacuum fluctuations of the input signal and the minimum noise added by the amplifier. The well-understood performance and the exceptional precision of this radiometer promise its applicability to a variety of problems such as verifying ground-state cooling in hybrid quantum systems [33,34] and upgrading microwave-cavity-based axion experiments [35–37].

Measurement setup.—Although employing a different physical system, our experiment pays tribute to a classic measurement setup in radio astronomy invented by R. H.

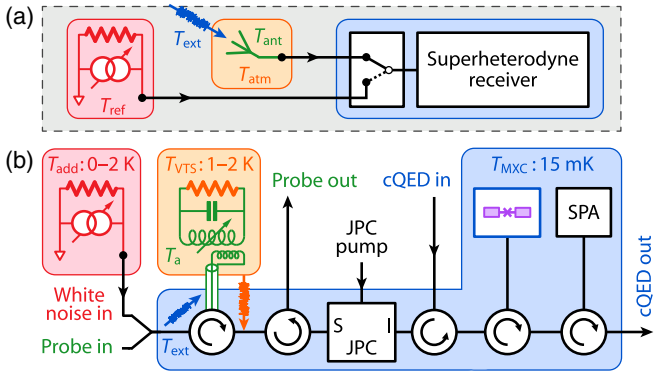

FIG. 1. (a) Diagram of an archetypal radio telescope. Blue box: radio receiver. Orange box: Earth's atmosphere. Green trident: receiving antenna. Blue arrow: extraterrestrial radiation. Red box: reference black-body radiator for temperature calibration. (b) Setup of our quantum microwave radiometric experiment. Blue area: mixing-chamber stage (MXC) of a dilution refrigerator. Orange box: variable-temperature stage (VTS), which is attached to the still stage of the same dilution refrigerator through a weak thermal link. Green transmission line: a niobium–titanium superconducting coaxial cable inductively coupled to a tunable antenna resonator (green). Blue arrow: residual thermal noise from the input line impinging on the resonator. Orange arrow: thermal leakage from the VTS to the MXC circuit due to the finite thermal conductivity along the interstage microwave wiring. Red box: tunable broadband noise generator. JPC: Josephson parametric converter with three ports: signal (S), idler (I), and pump. cQED: a transmon qubit (purple) dispersively coupled to a readout cavity (blue). SPA: superconducting nonlinear asymmetric inductive element parametric amplifier [41–43], which enables high-fidelity single-shot qubit readout.

Dicke and R. Beringer [38], whose block diagram is sketched in Fig. 1(a). Enclosed in blue is a microwave radiometer of the Dicke type [39], characterized by a two-way switch at the receiver input selecting between a black-body radiator at a reference temperature $T_{\rm ref}$ and a receiving antenna whose brightness temperature is a mixture of extraterrestrial radiation and atmospheric background: $T_{\rm ant} = \gamma T_{\rm atm} + (1-\gamma)T_{\rm ext}$, with γ denoting the atmospheric fractional absorption [40]. After calibrating $T_{\rm ant}$ using the reference radiator and separately measuring $T_{\rm atm}$ and γ, one can extract $T_{\rm ext}$—the microwave temperature of the astronomical object.

Our measurement setup is depicted in Fig. 1(b), with experimental parameters listed in Table S1 of the Supplemental Material [44]. At the system level, it can be viewed as a quantum-circuit realization of Dicke and Beringer's radio telescope. The analogy is highlighted by the color code. Our "antenna," with a tunable resonant frequency f_a and a mode temperature T_a, is a superconducting LC resonator [66] anchored to a variable-temperature stage (VTS), whose temperature $T_{\rm VTS}$ can be adjusted between 1–2 K without affecting other parts of the dilution refrigerator. The antenna mode is coupled with rate $\kappa_{a,i}$ to the internal dissipative bath at $T_{\rm VTS}$ and with rate $\kappa_{a,c}$ to a transmission line at $T_{\rm ext} \sim 0.1$ K [67]. Moreover, an external broadband noise generator is able to raise the temperature of the radiation on the transmission line by $T_{\rm add} = 0$–2 K. The combined variabilities of $T_{\rm VTS}$ and $T_{\rm add}$ allow various system parameters to be calibrated. In the quantum regime, i.e., $k_B T_j \lesssim h f_a$, with j denoting a mode or bath index, it is convenient to work with thermal photon populations in lieu of temperatures, which are linked by $\bar{n}_j = (e^{h f_a/k_B T_j} - 1)^{-1}$. The thermal population of the antenna mode is then given by

$$\bar{n}_a = \gamma \bar{n}_{\rm VTS} + (1-\gamma)(\bar{n}_{\rm ext} + \bar{n}_{\rm add}). \quad (1)$$

Here $\gamma := \kappa_{a,i}/(\kappa_{a,i} + \kappa_{a,c}) = \kappa_{a,i}/\kappa_a \sim 0.3$ is analogous to the "fractional absorption," which is measured by a network analyzer through the ports "Probe in" and "Probe out." During the experiment, $T_{\rm VTS}$ is continuously monitored by a calibrated thermometer. Therefore, the value of $\bar{n}_a$ can be computed once $T_{\rm ext}$ is obtained.

The detector of our quantum radiometer is a standard cQED module in the strong dispersive regime, where photon-number fluctuations in a 3D readout cavity [68] induce extra dephasing in a superconducting transmon qubit [69–71]. The intensity of the cavity field can then be deduced given its photon statistics. For instance, with broadband thermal noise at the cavity input, this photon-induced dephasing rate is given by [30]

$$\Gamma_{\rm th}(\bar{n}_r^{\rm th}) = {\rm Re}[(\kappa_r + i\chi)^2/4 + i\chi\kappa_r \bar{n}_r^{\rm th}]^{1/2} - \kappa_r/2, \quad (2)$$

where $\bar{n}_r^{\rm th}$ is the cavity thermal population, $\kappa_r = \kappa_{r,c} + \kappa_{r,i}$ is the cavity linewidth, and $\chi/2\pi$ is the dispersive shift of the qubit frequency per cavity photon. This dephasing rate can be measured via the Ramsey-fringe technique. Dispersive qubit readout [72] can be performed in reflection through the ports "cQED in" and "cQED out."

The cQED detector is only sensitive to incoming photons in the vicinity of the qubit-readout frequency f_r. To match it to the antenna resonator, a Josephson parametric converter (JPC) [73–75] is pumped at the frequency difference of its S and I ports and operated as a lossless microwave frequency converter [76] with a bandwidth ~100 MHz. Its conversion efficiency can be continuously adjusted from zero to unity. Without the pump, the JPC provides over 40 dB isolation between its S and I ports, protecting the qubit from antenna radiation during its initialization, manipulation, and readout.

Our quantum radiometer shows clear advantages over its classical counterpart in sensing microwave radiation in the quantum regime. First, by mapping the cavity population onto extra qubit dephasing, the cQED module directly measures the antenna radiation at the quantum level without passing it through any amplifier chain or demodulation circuit and without any sensitivity to vacuum noise.

The system noise is thus significantly suppressed. Second, as qubit dephasing is caused by photon-number fluctuations in the readout cavity, our detector essentially probes the excitations of an electromagnetic field instead of its quadrature amplitudes and is thus immune to the one-photon vacuum fluctuation, which is the inherent noise limit of classical radiometers with phase-preserving linear amplifiers [77–80]. These two factors contribute to the precision of the following experimental results.

Radiometry protocol.—Our radiometry measurements are based on the Ramsey-interferometry experiment [81,82]. As shown in Fig. 2(a), two $\pi/2$ qubit pulses

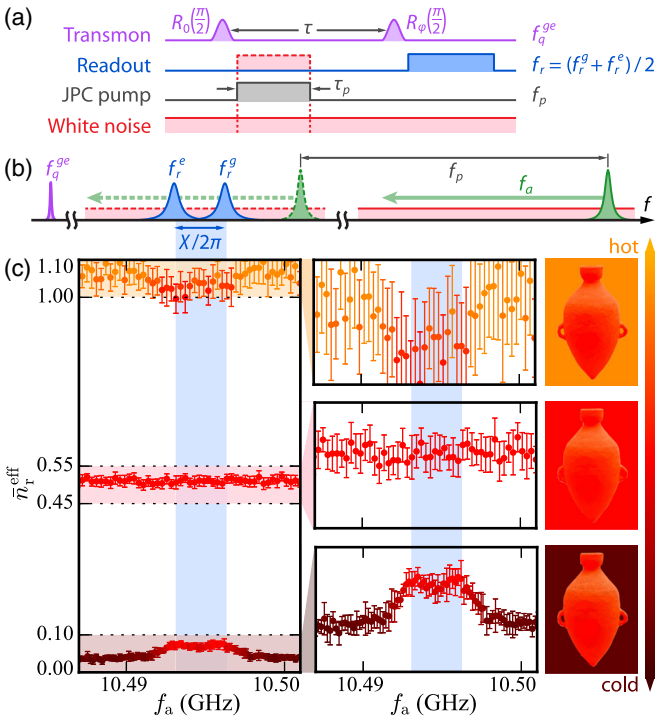

FIG. 2. (a) Pulse sequences for noise-induced dephasing measurements. For all datasets reported in this Letter, qubit rotations (purple) are completed in 200 ns; the second $\pi/2$ pulse is applied after the JPC pump (gray) by $\tau - \tau_p = 1$ μs; the single-shot qubit readout (blue) lasts for 1.08 μs. (b) Frequency landscape of the experiment. The solid green peak (right) belongs to the antenna resonator. The light green arrow indicates its frequency tunability. Along the frequency sweep, its down-converted image (dashed green peak) at $f_a - f_p$ at crosses the two resonances of the qubit-readout cavity (blue, $f_r^{g(e)} = f_r \pm \chi/4\pi$) separated by $\chi/2\pi$. The red floor refers to the added white noise. (c) Qubit-dephasing spectra at different added white-noise powers (from top to bottom, $\bar{n}_{\rm add}$ equal to 3.77, 1.66, and 0) showing the radiative heating, equilibrium, and cooling regimes, respectively. The blue ribbon stands for the range $f_r^e < f_a - f_p < f_r^g$. The accompanying sketches illustrate these regimes through an analogy based on pottery in a kiln—the color (temperature) contrasts between the amphorae and their backgrounds. For data in this subfigure, $\tau_p = 0.54$ μs and $T_{\rm VTS} = 1.03$ K.

are separated by a fixed delay τ. By varying their phase difference φ and projectively measuring the qubit state afterward, one can observe 2π-periodic Ramsey fringes with an amplitude equal to $\exp[-\int_0^\tau \Gamma(t)dt]/2$, in which $\Gamma(t)$ is the instantaneous qubit decoherence rate [44]. When the JPC is in the isolation mode, $\Gamma(t)$ equals the inherent Ramsey decoherence rate $\Gamma_{2R} = 1/T_{2R} = (4 \pm 0.3) \times 10^4$ s^{-1}. Conversely, when the JPC is in the full-conversion mode, antenna radiation enters the cQED circuit while the residual thermal photons at port I responsible for Γ_{2R} are redirected to the port S. (Here we assume that Γ_{2R} is solely caused by the residual photons coming from the "cQED in" port.) The ratio of the Ramsey amplitudes in these two circumstances equals $\exp[\int_0^\tau \Gamma_a(t)dt - \Gamma_{2R}\tau_p]$, in which $\Gamma_a(t)$ is the net dephasing rate induced by the antenna radiation, whose time dependence comes from the noninstantaneous response of the readout cavity, due to its finite linewidth, to the JPC pulse; τ_p is the duration of the JPC-conversion pump, which also limits the frequency resolution of the radiometry protocol to $\sim\tau_p^{-1}$. We can thus experimentally obtain an average dephasing rate $\bar{\Gamma}_a = \tau_p^{-1}\int_0^\tau \Gamma_a(t)dt$, in which the prefactor $1/\tau_p$ is chosen such that $\bar{\Gamma}_a = \Gamma_{\rm th}(\bar{n}_r^{\rm th})$ if the antenna radiation were steady-state white noise inducing an average cavity thermal population $\bar{n}_r^{\rm th}$ [83]. Finally, using Eq. (2), we link $\bar{\Gamma}_a$ to an *effective* cavity thermal population $\bar{n}_r^{\rm eff}$ as if the dephasing were induced by steady-state white noise. Note that instead of measuring the frequency shifts of the zero-crossing points of Ramsey fringes, our signal is the amplitude of the Ramsey fringes determined by measuring at the peaks, where shot noise vanishes in the absence of thermal photons or intrinsic qubit decoherence.

In practice, we choose $\tau_p \lesssim \min(T_{2R}, T_1)/10$ to both ensure sufficient resolution on $\bar{n}_r^{\rm eff}$ and mitigate qubit-relaxation events during the detection window. The statistical error bars of $\bar{\Gamma}_a$ and $\bar{n}_r^{\rm eff}$ contain contributions from both measurement imprecisions and the qubit T_1 fluctuations over time. The former scale as $1/\sqrt{N_{\rm rep}}$, where $N_{\rm rep}$ is the number of repetitions of the Ramsey sequence. In [44], we estimate the dynamic range of this radiometer to be ~50 dB.

Radiative cooling.—Following this protocol, we measured $\bar{n}_r^{\rm eff}$ while sweeping the frequency of the antenna resonator. Data are plotted in Fig. 2(c). When the down-converted antenna image is detuned from f_r^g and f_r^e, the qubit senses the white noise from the *external* bath with the thermal population $\bar{n}_{\rm ext} + \bar{n}_{\rm add}$ reflected by the antenna. When the antenna image is aligned with f_r^g or f_r^e, the qubit also senses the photons transmitted from the *internal* bath at $T_{\rm VTS} = 1.03$ K. As photons from a hotter bath lead to more qubit dephasing, three distinct regimes were observed: (i) If $T_{\rm add} = 0$, the dephasing increases when the resonances are aligned, indicating $T_{\rm ext} < T_{\rm VTS}$. (ii) If

$T_{\rm add} \approx 1$ K, the dephasing is independent of f_a, corresponding to $\bar{n}_{\rm ext} + \bar{n}_{\rm add} \approx \bar{n}_{\rm VTS}$. (iii) At any higher $T_{\rm add}$, the dephasing decreases when the resonances are aligned, suggesting $\bar{n}_{\rm ext} + \bar{n}_{\rm add} > \bar{n}_{\rm VTS}$. (i) and (iii) represent the radiative cooling and heating of the antenna mode by its external bath, respectively.

Our method for comparing $T_{\rm ext}$ and $T_{\rm VTS}$ by measuring thermal-photon-induced qubit dephasing is analogous to the disappearing-filament technique in pyrometry [84,85], which maps the high temperatures of quasiblack bodies onto visible colors. Illustrated by the sketches on the right of Fig. 2(c), the peaked, flat, and dipped dephasing spectra ($\bar{n}_r^{\rm eff}$ vs f_a curves) are associated with the amphorae [86] being brighter, hardly distinguishable, and darker compared to the background radiation, respectively. Similar to the incandescent color in a kiln, the qubit dephasing in a circuit QED system is essentially used as a temperature indicator. This analogy conveys the ubiquity of the radiative cooling phenomenon and its applications [87].

Noise analysis.—We model our radiometer using the signal-flow diagram in Fig. 3(a) when the JPC is in the full-conversion mode and write the photon flux per unit bandwidth at the input of the qubit-readout cavity as

$$\bar{n}_r^{\rm in}[f - f_a] = \bar{n}_a^{\rm out}[f - f_a] t_{\rm loss} + \bar{n}_{\rm loss}(1 - t_{\rm loss}), \quad (3)$$

where $\bar{n}_a^{\rm out}[f-f_a] = \bar{n}_{\rm VTS}(t_a[f-f_a] + t_{\rm leak}) + (\bar{n}_{\rm ext} + \bar{n}_{\rm add})(1 - t_a[f-f_a])$ refers to the output photon flux per unit bandwidth of the antenna resonator. In Eq. (3), the term proportional to $\bar{n}_{\rm loss}$ represents the noise added by the cables, connectors, and circulators between the resonator and the cQED module; the term containing $\bar{n}_{\rm VTS} t_{\rm leak}$ represents the thermal leakage from the VTS. Together with the shot noise associated with the inherent qubit decoherence, they constitute the system noise of the radiometer—the total noise at the output of the radiometer in the absence of input signals. Other terms, proportional to either t_a or $1 - t_a$, are associated with photons from the internal or external bath of the resonator. As derived in [44], the $\bar{n}_r^{\rm eff}$ in our experiment, measured from the qubit dephasing induced by the impinging photon flux $\bar{n}_r^{\rm in}$, is

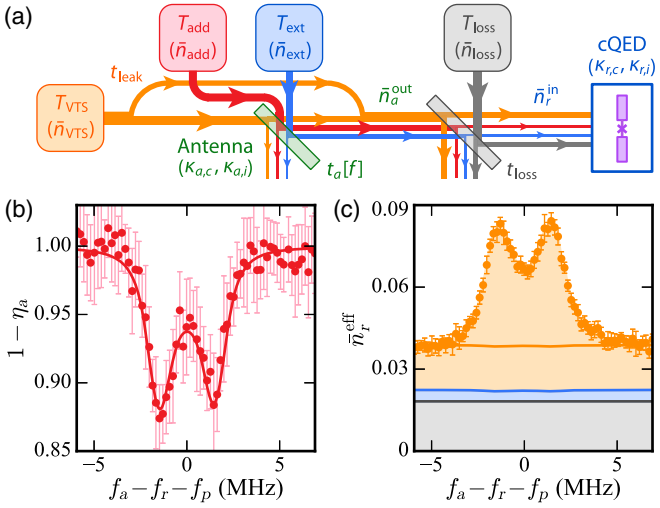

FIG. 3. (a) Noise model of the radiometer. Left beam splitter (green): tunable antenna resonator. Right beam splitter (gray): ohmic loss along the coaxial cables and circulators between the resonator and the cQED module. Their energy transmissivities are denoted as t_a and $t_{\rm loss}$. Four colored boxes represent the thermal baths. Yellow: internal bath in equilibrium with the VTS, whose thermal leakage to the MXC-stage circuits is represented by the transmissivity $t_{\rm leak}$. Red: white-noise source. Blue: external bath in the transmission line. Gray: dissipation between the antenna and the cQED cavity. (b) $1 - \eta_a$ and (c) $\bar{n}_r^{\rm eff}$ in the absence of added white noise at different antenna frequencies with $T_{\rm VTS} = 1.03$ K. The solid red curve in (b) is the theoretical prediction based on the experimental values of $\kappa_{a,c}$, $\kappa_{a,i}$, κ_r, and χ, with no fitting parameter. In (c), contributions of different baths are indicated using the same color code as that in (a). The orange line separates the VTS leakage (below) and the transmitted radiation from the resonator (above). For all data in this figure, $\tau_p = 1.08$ μs.

$$\begin{aligned}\bar{n}_r^{\rm eff}[f_r + f_p - f_a, \tau_p] = \{&\bar{n}_{\rm VTS} t_{\rm loss} \eta_a[f_r + f_p - f_a, \tau_p] \\ &+ (\bar{n}_{\rm ext} + \bar{n}_{\rm add}) t_{\rm loss}(1 - \eta_a[f_r + f_p - f_a, \tau_p]) \\ &+ \bar{n}_{\rm loss}(1 - t_{\rm loss}) + \bar{n}_{\rm VTS} t_{\rm leak} t_{\rm loss}\} \kappa_r^{-2} \kappa_{r,c} \kappa_a, \end{aligned} \quad (4)$$

in which the dimensionless η_a is the ratio of the qubit dephasing induced by a filtered thermal bath to that induced by the same bath without a Lorentzian antenna.

In Fig. 3(b), we plot the experimental data of η_a together with our theoretical predictions (see the Supplemental Material [44] for details). The noise calibration results are shown in Table I, where the system noise is given by $\bar{n}_{\rm sys} = \bar{n}_{\rm para} + \bar{n}_{\rm shot}$, in which $\bar{n}_{\rm para} := \bar{n}_{\rm VTS} t_{\rm leak} + \bar{n}_{\rm loss}(1 - t_{\rm loss})/t_{\rm loss}$ denotes the parasitic white noise referred to the antenna input, and $\bar{n}_{\rm shot}$, derived in [44], is the shot noise due to the inherent qubit decoherence. We obtain $\bar{n}_{\rm sys} = 0.25 \pm 0.02$ and $T_{\rm sys} = (0.31 \pm 0.01)$ K $\sim hf/2k_B$ [88]. Radiative cooling is manifested again through $\bar{n}_{\rm ext} \sim \bar{n}_{\rm VTS}/100$ and $\bar{n}_a \sim \bar{n}_{\rm VTS}/3$. Viewed from the point of photon counting, the performance of our qubit radiometer is comparable to state-of-the-art microwave single-photon detectors in the limit of small input-photon numbers (see the Supplemental Material [44] for details).

TABLE I. Noise parameters. The values of $\bar{n}_{\mathrm{para}}$, $\bar{n}_{\mathrm{sys}}$, and $\bar{n}_a$ (T_a) are based on $T_{\mathrm{VTS}} = 1.03$ K ($\bar{n}_{\mathrm{VTS}} = 1.59$). $t_{\mathrm{leak}} = 0.046 \pm 0.005$; $t_{\mathrm{loss}} = 0.52 \pm 0.06$.

$\bar{n}_{\mathrm{loss}}$	$\bar{n}_{\mathrm{ext}}$	$\bar{n}_{\mathrm{para}}$	$\bar{n}_a$
0.09 ± 0.01	0.014 ± 0.005	0.16 ± 0.02	0.49 ± 0.01

Prospect.—Two applications are within sight: First, our setup can be used to study the thermodynamics of hybrid quantum systems, such as verifying the ground-state cooling of an electro-optomechanical photon converter [33] or a spin ensemble [34]. Second, superconducting qubits have been envisaged to replace low-noise amplifiers as itinerant photon detectors in microwave-cavity-based axion experiments [35–37]. Considering the resemblance of our measurement setup to an axion detector [89–91], this radiometry protocol is useful for detecting this hypothetical particle and constraining theories of dark matter.

We acknowledge V. V. Sivak for fabricating the SNAIL parametric amplifier, and P. Bertet, A. A. Clerk, L. DiCarlo, Liang Jiang, S. K. Lamoreaux, K. W. Lehnert, and Andreas Wallraff for insightful discussions. Z. W. thanks P. Reinhold and S. O. Mundhada for their assistance on FPGA electronics. Use of facilities was supported by the Yale Institute for Nanoscience and Quantum Engineering and the Yale School of Engineering and Applied Science clean room. This research was supported by the U.S. Army Research Office (Grants No. W911NF-18-1-0020 and No. W911NF-18-1-0212), the U.S. Air Force Office of Scientific Research (Grant No. FA9550-15-1-0029), and the National Science Foundation (Grant No. DMR-1609326).

*Corresponding author.
zhixin.wang@yale.edu
†Corresponding author.
michel.devoret@yale.edu
‡Present address: Argonne National Laboratory, Lemont, Illinois 60439, USA.
§Present address: Department of Electrical and Computer Engineering, University of Texas, Austin, Texas 78758, USA.

[1] W. Herschel, Phil. Trans. R. Soc. London **90**, 284 (1800).
[2] P. L. Dulong and A. T. Petit, *Recherches sur la mesure des températures et sur les lois de la communication de la chaleur* (Imprimerie royale, Paris, 1818).
[3] J. Tyndall, *On Radiation: The "Rede" Lecture* (Longman, London, 1865).
[4] O. Lummer and E. Pringsheim, Verh. Dtsch. Phys. Ges. **2**, 163 (1900), https://archive.org/details/verhandlungende01goog/page/n172.
[5] H. Rubens and F. Kurlbaum, Sitzungsber. Preuss. Akad. Wiss. Phys. Math. Kl. **41**, 929 (1900), https://www.biodiversitylibrary.org/item/125575#page/248/mode/1up.
[6] A. A. Penzias and R. W. Wilson, Astrophys. J. **142**, 419 (1965).
[7] P. G. Roll and D. T. Wilkinson, Phys. Rev. Lett. **16**, 405 (1966).
[8] T. F. Howell and J. R. Shakeshaft, Nature (London) **210**, 1318 (1966).
[9] Y. M. Blanter and M. Büttiker, Phys. Rep. **336**, 1 (2000).
[10] P. W. Graham, I. G. Irastorza, S. K. Lamoreaux, A. Lindner, and K. A. van Bibber, Annu. Rev. Nucl. Part. Sci. **65**, 485 (2015).
[11] N. Skou and D. Le Vine, *Microwave Radiometer Systems: Design and Analysis*, 2nd ed. (Artech House, Norwood, Massachusetts, 2006).
[12] The sensitivity of a total-power radiometer is written as $\delta T = T_{\mathrm{sys}}\sqrt{(B\tau_{\mathrm{int}})^{-1} + (\delta G/G)^2}$, in which τ_{int} is the integration time, B is the detection bandwidth, and G and δG are the receiver gain and its fluctuation.
[13] E. W. Bryerton, M. Morgan, and M. W. Pospieszalski, in *2013 IEEE Radio and Wireless Symposium, Austin* (2013), pp. 358–360, https://dx.doi.org/10.1109/RWS.2013.6486740.
[14] N. Jarosik, C. L. Bennett, M. Halpern, G. Hinshaw, A. Kogut, M. Limon, S. S. Meyer, L. Page, M. Pospieszalski, D. N. Spergel, G. S. Tucker, D. T. Wilkinson, E. Wollack, E. L. Wright, and Z. Zhang, Astrophys. J. Suppl. Ser. **145**, 413 (2003).
[15] B. Aja, E. Artal, L. de la Fuente, J. P. Pascual, A. Mediavilla, N. Roddis, D. Kettle, W. F. Winder, L. P. Cara, and P. de Paco, IEEE Trans. Microwave Theory Tech. **53**, 2050 (2005).
[16] A. Blais, R.-S. Huang, A. Wallraff, S. M. Girvin, and R. J. Schoelkopf, Phys. Rev. A **69**, 062320 (2004).
[17] A. Blais, J. Gambetta, A. Wallraff, D. I. Schuster, S. M. Girvin, M. H. Devoret, and R. J. Schoelkopf, Phys. Rev. A **75**, 032329 (2007).
[18] R. J. Schoelkopf and S. M. Girvin, Nature (London) **451**, 664 (2008).
[19] S. M. Girvin, in *Quantum Machines: Measurement and Control of Engineered Quantum Systems*, Lecture Notes of the Les Houches Summer School, Session XCVI, edited by M. Devoret, B. Huard, R. Schoelkopf, and L. F. Cugliandolo (Oxford University Press, Oxford, 2014), pp. 113–255.
[20] D. I. Schuster, A. Wallraff, A. Blais, L. Frunzio, R.-S. Huang, J. Majer, S. M. Girvin, and R. J. Schoelkopf, Phys. Rev. Lett. **94**, 123602 (2005).
[21] P. Bertet, I. Chiorescu, G. Burkard, K. Semba, C. J. P. M. Harmans, D. P. DiVincenzo, and J. E. Mooij, Phys. Rev. Lett. **95**, 257002 (2005).
[22] C. Rigetti, J. M. Gambetta, S. Poletto, B. L. T. Plourde, J. M. Chow, A. D. Córcoles, J. A. Smolin, S. T. Merkel, J. R. Rozen, G. A. Keefe, M. B. Rothwell, M. B. Ketchen, and M. Steffen, Phys. Rev. B **86**, 100506(R) (2012).
[23] A. P. Sears, A. Petrenko, G. Catelani, L. Sun, H. Paik, G. Kirchmair, L. Frunzio, L. I. Glazman, S. M. Girvin, and R. J. Schoelkopf, Phys. Rev. B **86**, 180504(R) (2012).
[24] F. Yan, S. Gustavsson, A. Kamal, J. Birenbaum, A. P. Sears, D. Hover, T. J. Gudmundsen, D. Rosenberg, G. Samach, S. Weber, J. L. Yoder, T. P. Orlando, J. Clarke, A. J. Kerman, and W. D. Oliver, Nat. Commun. **7**, 12964 (2016).
[25] F. Yan, D. Campbell, P. Krantz, M. Kjaergaard, D. Kim, J. L. Yoder, D. Hover, A. Sears, A. J. Kerman, T. P. Orlando,

S. Gustavsson, and W. D. Oliver, Phys. Rev. Lett. **120**, 260504 (2018).
[26] J.-H. Yeh, J. LeFebvre, S. Premaratne, F. C. Wellstood, and B. S. Palmer, J. Appl. Phys. **121**, 224501 (2017).
[27] Z. Wang, S. Shankar, Z. K. Minev, P. Campagne-Ibarcq, A. Narla, and M. H. Devoret, Phys. Rev. Applied **11**, 014031 (2019).
[28] P. Bertet, I. Chiorescu, C. J. P. M. Harmans, and J. E. Mooij, arXiv:cond-mat/0507290.
[29] J. Gambetta, A. Blais, D. I. Schuster, A. Wallraff, L. Frunzio, J. Majer, M. H. Devoret, S. M. Girvin, and R. J. Schoelkopf, Phys. Rev. A **74**, 042318 (2006).
[30] A. A. Clerk and D. W. Utami, Phys. Rev. A **75**, 042302 (2007).
[31] D. Brunt, Q. J. R. Meteorol. Soc. **58**, 389 (1932).
[32] P. Groen, J. Meteorol. **4**, 63 (1947).
[33] C. Zhong, Z. Wang, C. Zou, M. Zhang, X. Han, W. Fu, M. Xu, S. Shankar, M. H. Devoret, H. X. Tang, and L. Jiang, Phys. Rev. Lett. **124**, 010511 (2020).
[34] B. Albanese, S. Probst, V. Ranjan, C. W. Zollitsch, M. Pechal, A. Wallraff, J. J. L. Morton, D. Vion, D. Esteve, E. Flurin, and P. Bertet, Nat. Phys. **16**, 751 (2020).
[35] S. K. Lamoreaux, K. A. van Bibber, K. W. Lehnert, and G. Carosi, Phys. Rev. D **88**, 035020 (2013).
[36] H. Zheng, M. Silveri, R. T. Brierley, S. M. Girvin, and K. W. Lehnert, arXiv:1607.02529.
[37] A. Dixit, A. Chou, and D. Schuster, in Microwave Cavities and Detectors for Axion Research, *Springer Proceedings in Physics 211*, edited by G. Carosi, G. Rybka, and K. van Bibber (Springer, Cham, 2018), pp. 97–103.
[38] R. H. Dicke and R. Beringer, Astrophys. J. **103**, 375 (1946).
[39] R. H. Dicke, Rev. Sci. Instrum. **17**, 268 (1946).
[40] R. H. Dicke, R. Beringer, R. L. Kyhl, and A. B. Vane, Phys. Rev. **70**, 340 (1946).
[41] N. E. Frattini, U. Vool, S. Shankar, A. Narla, K. M. Sliwa, and M. H. Devoret, Appl. Phys. Lett. **110**, 222603 (2017).
[42] N. E. Frattini, V. V. Sivak, A. Lingenfelter, S. Shankar, and M. H. Devoret, Phys. Rev. Applied **10**, 054020 (2018).
[43] V. V. Sivak, N. E. Frattini, V. R. Joshi, A. Lingenfelter, S. Shankar, and M. H. Devoret, Phys. Rev. Applied **11**, 054060 (2019).
[44] See Supplemental Material, which includes Refs. [45–65], at http://link.aps.org/supplemental/10.1103/PhysRevLett.126.180501 for further experimental details and theoretical analysis of this work.
[45] C. Rigetti, Quantum gates for superconducting qubits, Ph.D. dissertation, Yale University, 2009.
[46] F. Lecocq, I. M. Pop, Z. Peng, I. Matei, T. Crozes, T. Fournier, C. Naud, W. Guichard, and O. Buisson, Nanotechnology **22**, 315302 (2011).
[47] K. Serniak, S. Diamond, M. Hays, V. Fatemi, S. Shankar, L. Frunzio, R. J. Schoelkopf, and M. H. Devoret, Phys. Rev. Applied **12**, 014052 (2019).
[48] E. Flurin, The Josephson mixer: A swiss army knife for microwave quantum optics, Ph.D. dissertation, École normale supérieure, 2014.
[49] K. Sliwa, Improving the quality of heisenberg back-action of qubit measurements made with parametric amplifiers, Ph.D. dissertation, Yale University, 2016.
[50] A. B. Zorin, Phys. Rev. Applied **6**, 034006 (2016).
[51] M. Silveri, E. Zalys-Geller, M. Hatridge, Z. Leghtas, M. H. Devoret, and S. M. Girvin, Phys. Rev. A **93**, 062310 (2016).
[52] A. A. Clerk, M. H. Devoret, S. M. Girvin, F. Marquardt, and R. J. Schoelkopf, Rev. Mod. Phys. **82**, 1155 (2010).
[53] D. F. Walls and G. J. Milburn, *Quantum Optics*, 2nd ed. (Springer, Berlin and Heidelberg, 2008).
[54] M. O. Scully and M. S. Zubairy, *Quantum Optics* (Cambridge University Press, Cambridge, England, 1997).
[55] M. Xu, X. Han, C.-L. Zou, W. Fu, Y. Xu, C. Zhong, L. Jiang, and H. X. Tang, Phys. Rev. Lett. **124**, 033602 (2020).
[56] K. Inomata, Z. Lin, K. Koshino, W. D. Oliver, J.-S. Tsai, T. Yamamoto, and Y. Nakamura, Nat. Commun. **7**, 12303 (2016).
[57] S. Kono, K. Koshino, Y. Tabuchi, A. Noguchi, and Y. Nakamura, Nat. Phys. **14**, 546 (2018).
[58] R. Lescanne, S. Deléglise, E. Albertinale, U. Réglade, T. Capelle, E. Ivanov, T. Jacqmin, Z. Leghtas, and E. Flurin, Phys. Rev. X **10**, 021038 (2020).
[59] A. Narla, S. Shankar, M. Hatridge, Z. Leghtas, K. M. Sliwa, E. Zalys-Geller, S. O. Mundhada, W. Pfaff, L. Frunzio, R. J. Schoelkopf, and M. H. Devoret, Phys. Rev. X **6**, 031036 (2016).
[60] P. Campagne-Ibarcq, E. Zalys-Geller, A. Narla, S. Shankar, P. Reinhold, L. Burkhart, C. Axline, W. Pfaff, L. Frunzio, R. J. Schoelkopf, and M. H. Devoret, Phys. Rev. Lett. **120**, 200501 (2018).
[61] J.-C. Besse, S. Gasparinetti, M. C. Collodo, T. Walter, P. Kurpiers, M. Pechal, C. Eichler, and A. Wallraff, Phys. Rev. X **8**, 021003 (2018).
[62] L. Zhong, S. Al Kenany, K. M. Backes, B. M. Brubaker, S. B. Cahn, G. Carosi, Y. V. Gurevich, W. F. Kindel, S. K. Lamoreaux, K. W. Lehnert *et al.*, Phys. Rev. D **97**, 092001 (2018).
[63] R. D. Peccei and H. R. Quinn, Phys. Rev. Lett. **38**, 1440 (1977).
[64] M. S. Hersman and G. A. Poe, IEEE Trans. Microwave Theory Tech. **29**, 32 (1981).
[65] D. F. Wait, J. Res. Natl. Bur. Stand. **71C**, 127 (1967).
[66] M. Xu, X. Han, W. Fu, C.-L. Zou, M. H. Devoret, and H. X. Tang, Appl. Phys. Lett. **114**, 192601 (2019).
[67] T_{ext} is in principle set by the temperature of the base attenuator on the "Probe in" line. In practice, for the purpose of a parallel experiment, this 30 dB cryogenic attenuator is anchored to another variable-temperature stage (VTS) similar to the one holding the tunable antenna resonator but connected to the 15 mK mixing-chamber stage through a weak thermal link. When the external noise generator is turned off, the ruthenium-oxide thermometer on the mixing-chamber VTS reads 70 mK. Considering extra noise added by the following circulators and superconducting cables, we estimate $T_{\mathrm{ext}} \sim 0.1$ K, which is consistent with the radiometric data.
[68] H. Paik, D. I. Schuster, L. S. Bishop, G. Kirchmair, G. Catelani, A. P. Sears, B. R. Johnson, M. J. Reagor, L. Frunzio, L. I. Glazman, S. M. Girvin, M. H. Devoret, and R. J. Schoelkopf, Phys. Rev. Lett. **107**, 240501 (2011).
[69] A. Cottet, Implementation of a quantum bit in a superconducting circuit, Ph.D. dissertation, Université Paris VI, 2002.

[70] J. Koch, T. M. Yu, J. Gambetta, A. A. Houck, D. I. Schuster, J. Majer, A. Blais, M. H. Devoret, S. M. Girvin, and R. J. Schoelkopf, Phys. Rev. A **76**, 042319 (2007).
[71] J. A. Schreier, A. A. Houck, J. Koch, D. I. Schuster, B. R. Johnson, J. M. Chow, J. M. Gambetta, J. Majer, L. Frunzio, M. H. Devoret, S. M. Girvin, and R. J. Schoelkopf, Phys. Rev. B **77**, 180502(R) (2008).
[72] A. Narla, Flying qubit operations in superconducting circuits, Ph.D. dissertation, Yale University, 2017.
[73] N. Bergeal, R. Vijay, V. E. Manucharyan, I. Siddiqi, R. J. Schoelkopf, S. M. Girvin, and M. H. Devoret, Nat. Phys. **6**, 296 (2010).
[74] N. Bergeal, F. Schackert, M. Metcalfe, R. Vijay, V. E. Manucharyan, L. Frunzio, D. E. Prober, R. J. Schoelkopf, S. M. Girvin, and M. H. Devoret, Nature (London) **465**, 64 (2010).
[75] N. Roch, E. Flurin, F. Nguyen, P. Morfin, P. Campagne-Ibarcq, M. H. Devoret, and B. Huard, Phys. Rev. Lett. **108**, 147701 (2012).
[76] B. Abdo, K. Sliwa, F. Schackert, N. Bergeal, M. Hatridge, L. Frunzio, A. D. Stone, and M. Devoret, Phys. Rev. Lett. **110**, 173902 (2013).
[77] J. R. Tucker and M. J. Feldman, Rev. Mod. Phys. **57**, 1055 (1985).
[78] L. P. Bolgiano, IRE Trans. Microwave Theory Tech. **9**, 315 (1961).
[79] H. Heffner, Proc. IRE **50**, 1604 (1962).
[80] C. M. Caves, Phys. Rev. D **26**, 1817 (1982).
[81] N. F. Ramsey, Phys. Rev. **78**, 695 (1950).
[82] D. Vion, A. Aassime, A. Cottet, P. Joyez, H. Pothier, C. Urbina, D. Esteve, and M. H. Devoret, Science **296**, 886 (2002).
[83] Intuitively, the reason for choosing an integral limit τ larger than the inverse of the prefactor $1/\tau_p$ can be understood by considering the time dynamics of the readout cavity as response to the JPC pulse: During the cavity ring-up and ring-down, the cavity photon population is lower than the steady-state response. The latter is only approximately reached at the end of the JPC pulse. Therefore, the dephasing caused by a pulsed white thermal noise during τ is asymptomatically equal to that caused by a steady-state white thermal noise during τ_p. A detailed proof can be found in Sec. V A of the Supplemental Material [44].
[84] L. Holborn and F. Kurlbaum, Ann. Phys. (Berlin) **315**, 225 (1903).
[85] L. Michalski, K. Eckersdorf, J. Kucharski, and J. McGhee, *Temperature Measurement*, 2nd ed. (Wiley, Chichester, West Sussex, 2001), p. 163.
[86] These drawings are based on an artifact in the collection of the Museum of Fine Arts in Boston. Amphorae of this shape are representative of the Yangshao culture (Banpo phase) in Neolithic China, c. 5000–4000 BCE.
[87] To cross-check the above results, we performed a separate classical radiometry experiment by probing the power at "Probe out" with a commercial spectrum analyzer. As explained in the Supplemental Material [44], the agreement between the data and the theory that assumes a constant $T_{\mathrm{VTS}} = 1.03$ K confirms the internal bath was not influenced while the external bath was being heated by the white-noise source. Therefore, readouts of the VTS thermometer can be reliably used in the calibration procedure of the radiometer.
[88] In comparison, the classical radiometry experiment performed with the same physical setup using a quantum-limited parametric amplifier yields $\bar{n}_{\mathrm{ext}}^{\mathrm{cl}} = 0.02^{+0.06}_{-0.02}$ and $T_{\mathrm{sys}}^{\mathrm{cl}} = (1.02 \pm 0.01)\ \mathrm{K} \sim 2hf/k_B$ (see Ref. [55]).
[89] S. J. Asztalos, G. Carosi, C. Hagmann, D. Kinion, K. van Bibber, M. Hotz, L. J. Rosenberg, G. Rybka, J. Hoskins, J. Hwang, P. Sikivie, D. B. Tanner, R. Bradley, and J. Clarke, Phys. Rev. Lett. **104**, 041301 (2010).
[90] N. Du *et al.* (ADMX Collaboration), Phys. Rev. Lett. **120**, 151301 (2018).
[91] B. M. Brubaker, L. Zhong, Y. V. Gurevich, S. B. Cahn, S. K. Lamoreaux, M. Simanovskaia, J. R. Root, S. M. Lewis, S. Al Kenany, K. M. Backes *et al.*, Phys. Rev. Lett. **118**, 061302 (2017).